Broad wavelength coverage 2.3 μm III-V-on-silicon DFB laser array

Markus-Christian Amann,[3] and Gunther Roelkens[1,2]

[1]Photonics Research Group, Ghent University-imec, Technologiepark-Zwijnaarde 15, B-9052 Ghent, Belgium
[2]Center for Nano- and Biophotonics (NB-Photonics), Ghent University, B-9052 Ghent, Belgium
[3]Walter Schottky Institut, Technische Universität München, Am Coulombwall 4, 85748 Garching, Germany
*Corresponding author: Ruijun.Wang@ugent.be

Received 17 March 2017; revised 16 July 2017; accepted 16 July 2017 (Doc. ID 290821); published 10 August 2017

Silicon photonics is a promising integrated-optics platform for optical communication and sensing applications. Integrating 2–3 μm wavelength widely tunable lasers on silicon photonic integrated circuits enables fully integrated spectroscopic sensors with different potential applications such as multi-species trace gas spectroscopy and bio-molecule detection. Here, we demonstrate a continuous-wave (CW) operated III–V-on-silicon distributed feedback (DFB) laser array covered a broad wavelength range from 2.28 to 2.43 μm. CW operation up to 25°C and an on-chip output power of 2.7 mW in a single mode at 5°C is achieved for lasers operating at 2.35 μm wavelength. Four-channel DFB laser arrays with a continuous tuning range of 10 nm and side mode suppression ratio of 40 dB over the whole range are also presented. This work is a major advance toward chip-scale silicon photonics spectroscopic sensing systems.

OCIS codes: (130.0130) Integrated optics; (130.3120) Integrated optics devices; (140.3490) Lasers, distributed-feedback.

https://doi.org/10.1364/OPTICA.4.000972

Gas sensing based on short-wave infrared and mid-infrared absorption spectroscopy has been proven to be a reliable technology for trace-gas measurements with fast response time and a high degree of specificity to the target gas [1,2]. However, most present optical sensors consist of discrete optical components and a bulk gas cell, which limits their viability for applications in portable and economical gas analysis. Integrated photonics platforms offer the potential to realize miniature and low-cost optical gas sensors [3–6]. As one of the most promising integrated photonics platforms, silicon photonics has been well-developed for optical communication applications during the past decade [7]. In recent years, its applications have been extended to sensing applications, including on-chip spectroscopic sensing [8]. Silicon photonics gas sensors that target different components have been demonstrated, including those that use, e.g., microring resonators [9,10] or spiral waveguides [11] to interact with the gas medium. In these gas sensors, the light from an external laser source is coupled into the silicon chip for the on-chip absorption spectroscopy measurement. The development of fully integrated silicon photonic integrated circuits (PICs) in the 2.3 μm wavelength range enable compact gas sensors with high sensitivity, since many important industrial gases (e.g., NH_3, CO, and CH_4) have strong absorption lines in this wavelength range [12]. It is also valuable for bio-sensing applications, such as non-invasive blood glucose measurements [8,13]. For a compact silicon photonics spectroscopic gas sensor, an integrated and tunable single-mode laser is the key component that should be developed. Recently, heterogeneously integrated III–V-on-silicon Fabry–Perot lasers around 2 μm were realized using strained InGaAs Type I heterostructures [14]. However, the emission wavelength range of laser sources based on the InP-based Type I material is limited to around 2.3 μm [15]. Recently, we demonstrated 2.3x μm heterogeneous III–V-on-silicon distributed feedback (DFB) laser sources based on an InP-based Type II heterostructure [16]. These lasers have been proven to be suitable for carbon monoxide gas detection using direct absorption spectroscopy, but the tuning range (by changing the driven current) of a single device is limited to 2 nm. The development of widely tunable silicon photonics laser sources in the 2–3 μm range enable to simultaneously detect several gases or broad absorption features of bio-molecules on a compact chip [17,18].

Mid-infrared DFB laser arrays have been realized on a III–V substrate at wavelengths beyond 4 μm based on quantum cascade structures [19]. These arrays attract great interest for gas sensing applications [20]. However, 2–4 μm range DFB laser arrays and further integrating the arrays on a PIC still need to be demonstrated. In this paper we report, to the best our knowledge, the first broad wavelength coverage DFB laser array in the 2 μm wavelength range, which is realized on a heterogeneous III–V-on-silicon platform and uses a W-shaped InGaAs/GaAsSb Type II active region. In continuous-wave (CW) regime, the laser array can cover a wavelength range of 150 nm (2.28–2.43 μm), which exceeds the wavelength coverage (~120 nm) of a recently demonstrated 2.3 μm GaSb-based external cavity laser based on a bulky Littrow configuration [21]. By varying

the laser drive current, 10 nm continuous tuning is achieved using four DFB lasers with the same DFB grating period but different III–V waveguide widths.

The DFB laser arrays are fabricated on the heterogeneous III–V-on-silicon device platform developed for optical communication and sensing [22]. An InP-based Type II epitaxial layer stack with an active region consisting of six periods of a W-shaped InGaAs/GaAsSb quantum well is used. Detailed information of the active region design can be found in Ref. [23]. The photoluminescence (PL) peak of the active region is located around 2.33 μm, so that the gain spectrum can overlap the absorption window of e.g., NH_3, CO, and CH_4. The silicon PIC is patterned by 193 nm deep UV lithography, followed by a 180 nm deep dry etch in a 400 nm thick silicon device layer to define the silicon waveguides and gratings. Then the wafer is planarized by SiO_2 deposition, followed by chemical mechanical polishing (CMP) down to the silicon waveguide. After the silicon process, the InP-based epitaxial layer stack is adhesively bonded to the fabricated silicon PIC using a 50 nm thick divinylsiloxane-bis-benzocyclobutene (DVS-BCB) bonding layer. Afterward, the InP substrate is removed by HCl wet etching. Then the III–V mesa of the laser diode is processed on the III–V membrane. A schematic picture of the III–V-on-silicon DFB laser array is shown in Fig. 1(a). The fabricated DFB laser consists of a gain section in the center and a III–V/silicon spot size converter (SSC) on both sides. The light is coupled from the gain section to the silicon waveguides through the III–V/silicon SSCs. A quarter-wave-shifted first-order DFB silicon grating is defined underneath the gain section. A common *p*-contact pad is used, which also acts as a heat spreader for the laser array. Figure 1(b) shows a scanning electron microscopy (SEM) image of the longitudinal cross section of the fabricated devices. The device cross section is similar to that shown in Ref. [16], but thinner DVS-BCB is used in the DFB laser arrays presented in this paper. The smaller gap between the active region and the DFB grating leads to a stronger coupling. When the III–V mesa width is 5 μm and DVS-BCB thickness is 50 nm, the coupling coefficient κ of the DFB grating is calculated to be 80 cm^{-1}. More information about the device structure and fabrication can found in Refs. [16,24].

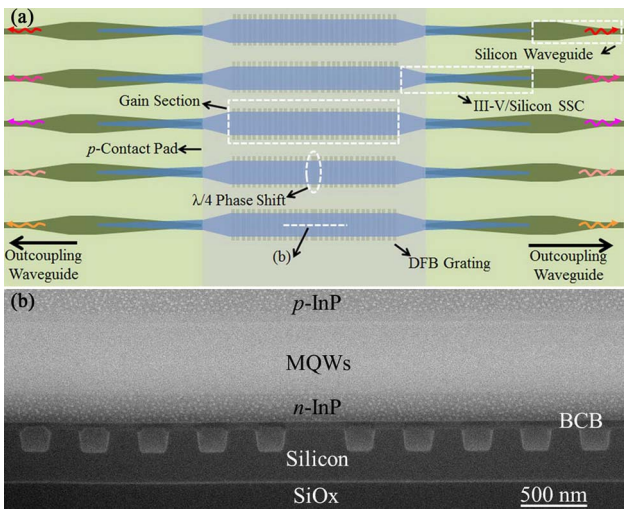

Fig. 1. (a) Schematic of the III–V-on-silicon DFB laser array. (b) SEM image of the longitudinal cross section of the gain section.

Fabricated laser arrays are mounted on a temperature-controlled stage during measurements. In the III–V-on-silicon PIC, silicon grating couplers are integrated with the laser devices for on-chip measurement. The light in the silicon waveguide is coupled out through the grating coupler and collected by a standard single-mode fiber (SMF-28), which is connected to an optical spectrum analyzer (OSA, Yokogawa AQ6375). The output power of the integrated lasers is determined by measuring the chip-to-fiber coupling efficiency of a grating coupler reference structure. The measured coupling efficiency is −10 dB at 2.35 μm with 150 nm 3 dB bandwidth. The current–voltage (I-V) and CW on-chip output power–current (L-I) characteristics of a laser with a grating pitch of 353 nm are shown in Fig. 2 at different heat-sink temperatures. The threshold current is 60 mA at 5°C and increases to 110 mA at room temperature. For a device with a 3.8 μm wide and 1000 μm long gain section, these threshold current values corresponds to current densities of 1.6 and 2.9 kA/cm^2, respectively. The inset shows the fiber-coupled emission spectra as a function of the bias current. The stop band width deduced from the spectrum is around 3.8 nm, so a normalized coupling coefficient κL of 7.5 is calculated. As seen in Fig. 2, the band edge mode starts lasing as the bias current increases to 185 mA at 5°C. In current region II (185–270 mA) marked in the inset, the DFB laser shows dual-mode operation. This is the result of spatial hole burning in the DFB laser due to the high normalized coupling coefficient κL. In current ranges I (60–185 mA) and III (270–350 mA), the DFB laser exhibits stable single-mode operation. Tuning ranges of 1.5 and 1.2 nm is achieved in these two current ranges, respectively. The maximum single-mode (SMSR > 20 dB) on-chip output power is 0.5 mW and 2.7 mW for the defect mode and band edge mode, respectively. In Supplement 1, we also show the L-I characteristics of the laser in pulsed regime. The characteristic temperature T_0 of the laser is fitted to be 34 K. Using the method described in Ref. [25], a thermal resistance of 87 K/W is extracted, which can be further reduced by using a thinner buried oxide or by connecting the top *p*-contact pad to the silicon substrate.

Figure 3 shows the normalized emission spectra and maximum single-mode output power (indicated by the stars) of six DFB lasers with silicon grating pitch ranging from 343 nm (Laser1) to 368 nm (Laser6). The lasers are 1000 μm long. A side-mode suppression ratio (SMSR) of 30 dB is achieved for all the lasers.

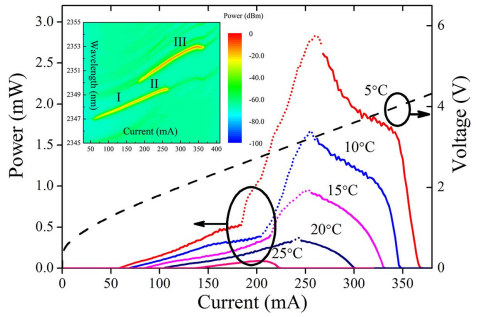

Fig. 2. CW light–current–voltage (L-I-V) characteristics of a heterogeneously integrated DFB laser with grating pitch of 353 nm at different heat-sink temperatures. The solid portions of the L-I curve indicate a single-mode emission with a SMSR of at least 20 dB, while the dashed portions correspond to dual-mode operation. The inset shows the spectral map of the laser device.

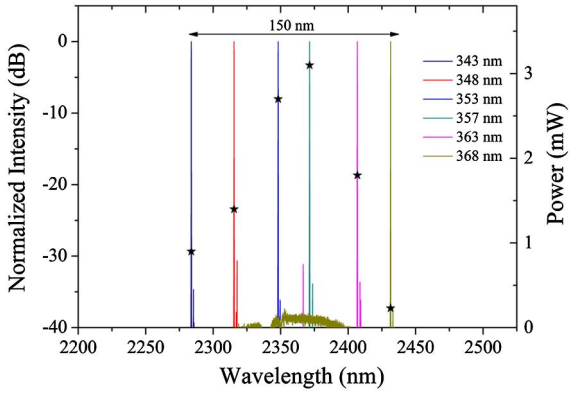

Fig. 3. Emission spectra and single-mode peak output power of six DFB lasers with different silicon grating pitch in an array. The widths of Laser1–Laser5 and Laser6 are 3.8 μm and 3.2 μm, respectively.

During measurements, all devices are driven in CW mode at a heat-sink temperature of 5°C, with 150 mA drive current for Laser1–Laser5 and 220 mA for Laser6. As the silicon grating pitch increases from 343 to 368 nm, the laser wavelength shifts from 2280 to 2430 nm. A 1 nm change in the DFB grating pitch results in ~6 nm shift in the lasing wavelength. The 150 nm lasing wavelength span overlaps with the absorption window of several important gases, including CH_4, CO, NH_3, C_2H_2, and HF. The maximum on-chip output power in single mode increases from 1 mW at 2280 nm to 3.1 mW at 2375 nm and reduces to 0.2 mW at 2430 nm. This trend matches the amplified spontaneous emission spectrum of the devices.

An effective way to get rid of the mode hopping between the defect mode and band edge mode in the DFB laser is to have a device with a lower κL. Here, we present the results of III–V-on-silicon lasers with a 5 μm wide and 700 μm long gain section, corresponding to $\kappa L = 5.6$. The CW L-I-V characteristics of a DFB laser with grating pitch of 353 nm are shown in Fig. 4(a). The threshold current is 62 mA (corresponding to a current density of 1.77 kA/cm^2) with a maximum on-chip output power of 1.8 mW at 190 mA at 5°C. In CW mode, the laser can operate close to room temperature. The inset of Fig. 4(a) shows the spectral map as a function of bias current at 5°C. A tuning range of more than 3 nm is achieved with a current-tuning coefficient of around 0.19 nm/mA. Single-mode lasing without mode hopping is observed in the whole CW operational current range (62–245 mA). With this shorter cavity length, a DFB laser array is also fabricated on the same silicon chip as the 1000 μm long one. Figure 4(b) shows the emission spectra of four DFB lasers biased at 150 mA at 5°C. All of these lasers have a 5 μm wide and 700 μm long gain section. The lasing wavelength shifts from 2290 to 2375 nm as the silicon grating pitch increases from 343 to 357 nm. The devices with grating pitch of 363 and 368 nm do not lase in CW mode at 5°C. This narrower wavelength span is attributed to the lower κL of the 700 μm long DFB lasers, which results in higher mirror loss. A SMSR above 43 dB is achieved for all devices.

The tuning range of an individual DFB laser by varying the bias current is limited to about 3 nm, as shown in the inset of Fig. 4(a). So the silicon grating pitch should be fabricated with 0.5 nm increments to get a continuously tunable DFB laser array, which is quite challenging for current silicon photonics pilot lines.

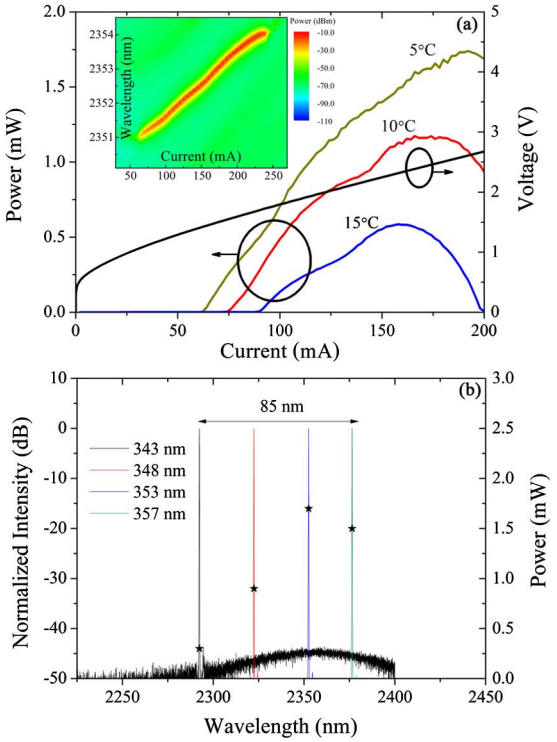

Fig. 4. (a) CW L-I-V plot of a heterogeneous InP-based Type II DFB laser with a 5 μm wide and 700 μm long gain section and grating pitch of 353 nm. The inset shows the evolution of the laser emission spectrum with increasing bias current at 5°C. (b) Normalized lasing spectra of four 700 μm long DFB lasers with a grating pitch ranging from 343 to 357 nm.

Another method to control the lasing wavelength is to adjust the modal index of the device. As the modal index is dependent on the width of III–V waveguide, which can be controlled using standard III–V contact lithography, a laser array with fine emission wavelength spacing (<3 nm) can be achieved by varying the gain section width. Figures 5(a) and 5(b) show the normalized lasing spectra as a function of the bias current for a four-wavelength DFB laser array with a 700 μm long gain section and a silicon grating pitches of 353 and 357 nm, respectively. The III–V gain section width varies from 3.8 to 6 μm while the width of the silicon DFB grating underneath is fixed at 8 μm. All of the lasers are driven in CW mode at 5°C. The wavelength spacing (~2.5 nm) of the lasers in each array is sufficiently small such that both arrays can continuously tune over a 10 nm wavelength range by varying the bias current. Laser arrays with much broader continuous-tuning range can be achieved by fabricating DFB gratings with a pitch step of 2 nm and varying the gain section width of five lasers with same grating pitch. In this way, in principle, more than 100 nm continuous wavelength coverage is possible. The corresponding laser output power as a function of the emission wavelength is shown in Supplement 1. Our results also suggest a method of accurately controlling the lasing wavelength of III–V-on-silicon DFB lasers by changing the III–V waveguide widths, which can be applied as well for the realization of dense wavelength-division-multiplexed laser arrays on silicon for optical communication applications.

In conclusion, we have demonstrated heterogeneously integrate III–V-on-silicon DFB laser arrays with broad wavelength

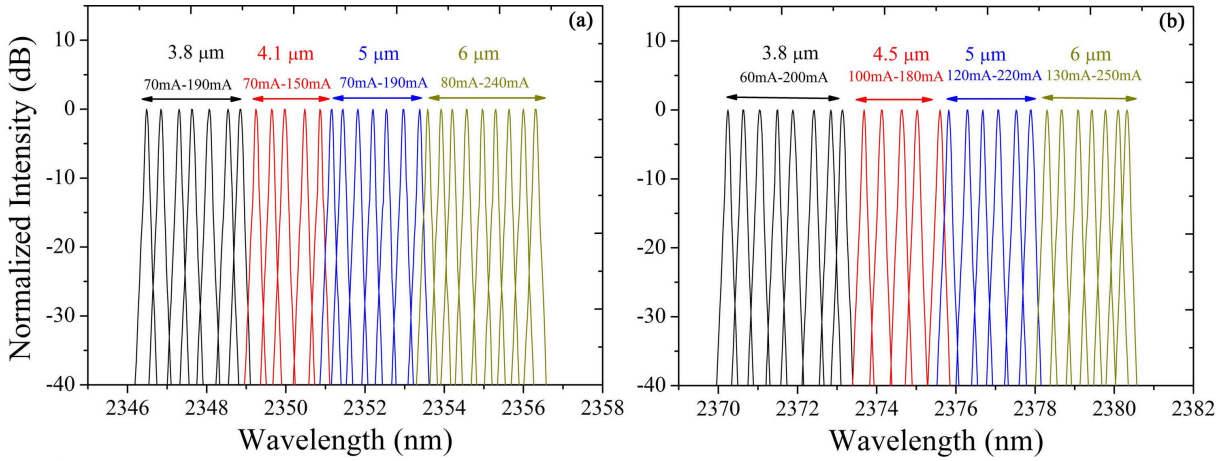

Fig. 5. Evolution of the lasing spectra as a function of the bias current (20 mA step) for four DFB lasers with different gain section widths and silicon grating pitches of (a) 353 nm and (b) 357 nm.

coverage by using InP-based Type II quantum wells as the gain section. With 1000 μm long gain sections, a CW-operated DFB laser array spanning the 2.28–2.43 μm wavelength range is obtained by varying the silicon grating pitch. As the III–V gain section length is reduced to 700 μm, we obtain a laser array with wavelength span of 85 nm, of which the individual lasers can be tuned continuously over 3 nm. By adjusting the III–V gain section width, two four-wavelength DFB arrays with 10 nm continuous tuning range are realized. The lasing wavelength range of the laser arrays overlaps with several important industrial gases, such as NH_3, CO, and CH_4. Therefore, the heterogeneous DFB laser arrays offer the potential to realize a fully integrated silicon photonics sensor that can simultaneously detect several gases.

Funding. H2020 European Research Council (ERC) (FireSpec, InSpectra, MIRACLE).

See Supplement 1 for supporting content.

REFERENCES

1. J. Hodgkinson and R. P. Tatam, Meas. Sci. Technol. **24**, 012004 (2013).
2. M. W. Sigrist, R. Bartlome, D. Marinov, J. M. Rey, D. E. Vogler, and H. Wächter, Appl. Phys. B **90**, 289 (2008).
3. S. Latkowski, A. Hänsel, P. J. van Veldhoven, D. D'Agostino, H. Rabbani-Haghighi, B. Docter, N. Bhattacharya, P. J. A. Thijs, H. P. M. M. Ambrosius, M. K. Smit, K. A. Williams, and E. A. J. M. Bente, Optica **3**, 1412 (2016).
4. R. Soref, Nat. Photonics **4**, 495 (2010).
5. A. Spott, J. Peters, M. L. Davenport, E. J. Stanton, C. D. Merritt, W. W. Bewley, I. Vurgaftman, C. S. Kim, J. R. Meyer, J. Kirch, L. J. Mawst, D. Botez, and J. E. Bowers, Optica **3**, 545 (2016).
6. A. Spott, J. Peters, M. L. Davenport, E. J. Stanton, C. Zhang, C. D. Merritt, W. W. Bewley, I. Vurgaftman, C. S. Kim, J. R. Meyer, J. Kirch, L. J. Mawst, D. Botez, and J. E. Bowers, Photonics **3**, 35 (2016).
7. L. Vivien and L. Pavesi, eds., *Handbook of Silicon Photonics* (Taylor & Francis, 2016).
8. A. Subramanian, E. M. P. Ryckeboer, A. Dhakal, F. Peyskens, A. Malik, B. Kuyken, H. Zhao, S. Pathak, A. Ruocco, A. De Groote, P. C. Wuytens, D. Martens, F. Leo, W. Xie, U. D. Dave, M. Muneeb, P. Van Dorpe, J. Van Campenhout, W. Bogaerts, P. Bienstman, N. Le Thomas, D. Van Thourhout, Z. Hens, G. Roelkens, and R. Baets, Photon. Res. **3**, B47 (2015).
9. J. T. Robinson, L. Chen, and M. Lipson, Opt. Express **16**, 4296 (2008).
10. T. H. Stievater, M. W. Pruessner, D. Park, W. S. Rabinovich, R. Andrew McGill, D. A. Kozak, R. Furstenberg, S. A. Holmstrom, and J. B. Khurgin, Opt. Lett. **39**, 969 (2014).
11. E. J. Zhang, L. Tombez, J. Orcutt, S. Kamlapurkar, G. Wysocki, and W. M. Green, *Conference on Lasers and Electro-Optics (CLEO)* (2016), paper SF2H.1.
12. L. S. Rothman, I. E. Gordon, Y. Babikov, A. Barbe, D. C. Benner, P. F. Bernath, M. Birk, L. Bizzocchi, V. Boudon, L. R. Brown, A. Campargue, K. Chance, E. A. Cohen, L. H. Coudert, V. M. Devi, B. J. Drouin, A. Fayt, J.-M. Flaud, R. R. Gamache, J. J. Harrison, J.-M. Hartmann, C. Hill, J. T. Hodges, D. Jacquemart, A. Jolly, J. Lamouroux, R. J. Le Roy, G. Li, D. A. Long, O. M. Lyulin, C. J. Mackie, S. T. Massie, S. Mikhailenko, H. S. P. Müller, O. V. Naumenko, A. V. Nikitin, J. Orphal, V. Perevalov, A. Perrin, E. R. Polovtseva, C. Richard, M. A. H. Smith, E. Starikova, K. Sung, S. Tashkun, J. Tennyson, G. C. Toon, V. G. Tyuterev, and G. Wagner, J. Quantum Spectrosc. Radiat. Transfer **130**, 4 (2013).
13. N. V. Alexeeva and M. A. Arnold, J. Diabetes Sci. Technol. **3**, 219 (2009).
14. A. Spott, M. Davenport, J. Peters, J. Bovington, M. J. R. Heck, E. J. Stanton, I. Vurgaftman, J. Meyer, and J. Bowers, Opt. Lett. **40**, 1480 (2015).
15. S. Sprengel, F. Demmerle, and M.-C. Amann, Semicond. Sci. Technol. **26**, 014032 (2016).
16. R. Wang, S. Sprengel, A. Malik, A. Vasiliev, G. Boehm, R. Baets, M.-C. Amann, and G. Roelkens, Appl. Phys. Lett. **109**, 221111 (2016).
17. B. L. Upschulte, D. M. Sonnenfroh, and M. G. Allen, Appl. Opt. **38**, 1506 (1999).
18. D. Weidmann, A. A. Kosterev, F. K. Tittel, N. Ryan, and D. McDonald, Opt. Lett. **29**, 1837 (2004).
19. P. Rauter and F. Capasso, Laser Photon. Rev. **9**, 452 (2015).
20. L. Bizet, R. Vallon, B. Parvitte, M. Brun, G. Maisons, M. Carras, and V. Zeninari, Appl. Phys. B **123**, 145 (2017).
21. K. Vizbaras, E. Dvinelis, I. Šimonytė, A. Trinkūnas, M. Greibus, R. Songaila, T. Žukauskas, M. Kaušylas, and A. Vizbaras, Appl. Phys. Lett. **107**, 011103 (2015).
22. G. Roelkens, A. Abassi, P. Cardile, U. Dave, A. de Groote, Y. de Koninck, S. Dhoore, X. Fu, A. Gassenq, N. Hattasan, Q. Huang, S. Kumari, S. Keyvaninia, B. Kuyken, L. Li, P. Mechet, M. Muneeb, D. Sanchez, H. Shao, T. Spuesens, A. Z. Subramanian, S. Uvin, M. Tassaert, K. van Gasse, J. Verbist, R. Wang, Z. Wang, J. Zhang, J. van Campenhout, X. Yin, J. Bauwelinck, G. Morthier, R. Baets, and D. van Thourhout, Photonics **2**, 969 (2015).
23. S. Sprengel, C. Grasse, P. Wiecha, A. Andrejew, T. Gruendl, G. Boehm, R. Meyer, and M. C. Amann, IEEE J. Sel. Top. Quantum Electron. **19**, 1900909 (2013).
24. R. Wang, S. Sprengel, G. Boehm, M. Muneeb, R. Baets, M. C. Amann, and G. Roelkens, Opt. Express **24**, 21081 (2016).
25. K. Doi, T. Shindo, J. Lee, T. Amemiya, N. Nishiyama, and S. Arai, IEEE J. Quantum Electron. **50**, 321 (2014).